Tectonophysics 590 (2013) 106–120

Contents lists available at SciVerse ScienceDirect

Tectonophysics

journal homepage: www.elsevier.com/locate/tecto

Along-strike structural variations in the Southern Patagonian Andes: Insights from physical modeling

Jeremías Likerman [a,b,*], Juan Francisco Burlando [a,c], Ernesto O. Cristallini [a,b], Matías C. Ghiglione [a,c]

[a] Consejo Nacional de Investigaciones Científicas y Técnicas (CONICET), Avda. Rivadavia 1917, CP C1033AAJ, Ciudad de Buenos Aires, Argentina
[b] Laboratorio de Modelado Geológico (LaMoGe), Instituto de Estudios Andinos Don Pablo Groeber, Universidad de Buenos Aires, Ciudad Universitaria, C1428EHA, Buenos Aires, Argentina
[c] Laboratorio de Tectónica Andina, Instituto de Estudios Andinos Don Pablo Groeber, Universidad de Buenos Aires, Departamento de Ciencias Geológicas, Buenos Aires, Argentina

ARTICLE INFO

Article history:
Received 13 June 2012
Received in revised form 17 January 2013
Accepted 22 January 2013
Available online 31 January 2013

Keywords:
Southern Patagonian Andes
Asymmetric rift
Analog modeling
Tectonic inversion
Transfer zones

ABSTRACT

The Southern Patagonian Andes between 48° and 53° SL offers a unique opportunity to study the results of orogenic growth superimposed over a previously rifted region. In this sector the northern Austral or Magallanes basin was affected by late to middle Jurassic extension followed by Late Cretaceous to Neogene tectonic compression. The resultant fold-thrust belt displays significant along-strike variations in width and lateral position of the structural domains that may be reflecting a first order control of the Jurassic extensional depocenters, as proposed in previous works. This hypothesis is tested using a series of scaled sandbox analog models involving the positive inversion of two adjacent depocenters with different extensional rates accommodated by a transfer fault. The correlation between structures in the Southern Patagonian Andes and the features in the model have important first order similarities supporting the theory of a positively inverted extensional basin with a previous history of southward increase in extension. Moreover structural cross-sections analyzed from field and seismic data have a geometry that is consistent with serial cross sections resulting from the models.

1. Introduction

The geometrical and time–space evolution of structures in positively inverted extensional basins have specific peculiarities that can be used to reveal their extensional origin. During their evolution, rift segments grow, interact and may link up to develop two main types of interaction relevant at the rift scale, relay ramps or accommodation zones and transfer faults (Gibbs, 1984; Larsen, 1988; Peacock et al., 2000; Stewart and Hancock, 1991). The former consists of broad areas of reoriented bedding between extensional structures and are a common type of 'soft linkage' interaction (Walsh and Watterson, 1991). On the other hand, the 'hard linkage' interaction occurs when a transfer fault is developed. These subvertical transtensive faults, strike at high angle and transfer displacement between two adjacent normal faults undergoing differential extension (Gibbs, 1984). The presence of preexisting structural geometries such as those described above, will affect the evolution of later compressional structures during basin inversion (Beauchamp, 2004). Transfer zones can work as mechanical boundaries between fault bounded blocks during the positive inversion of normal structures (Konstantinovskaya et al., 2007) developing typical geometries such as the lateral termination of folding (Beauchamp, 2004; Paton and Underhill, 2004).

The distribution of Gondwanaland Mesozoic pre-orogenic rifts constitute a first-order control that determines the along-strike structural variations associated with a grand scale geotectonic segmentation of the Andes (Jacques, 2003; Kley et al., 1999; Uliana et al., 1995). Although the relationship between the distribution of previous rifting and the development of thick skinned deformation is well known in the northern (Carrera et al., 2006; Kley and Monaldi, 2002) and southern Central Andes (Giambiagi, 2003; Ramos et al., 2004) it has not been extensively studied in the Southern Patagonian Andes. The Andean segment between 48° and 53° SL (Fig. 1), where the northern Austral or Magallanes basin develops, offers a unique opportunity to study the results of orogenic growth superimposed over a previously rifted region (Romans et al., 2009), and displays characteristics particular to this region (Fosdick et al., 2011; Ghiglione et al., 2009; Kraemer, 1998). One of the main differences is that the northern and southern Central Andes can each be divided into sectors with different Mesozoic histories and therefore contrasting end members of orogenic geometries (Kley and Monaldi, 2002; Ramos, 2006). On the contrary, the Southern Patagonian Andes underwent a similar geological history with an overall north to south regional increase in Jurassic stretching that exerted a strong control on subsequent sedimentation (Fildani and Hessler, 2005; Fildani et al., 2003; Romans et al., 2009; Wilson, 1991) and accordingly it shows lateral variations in the structural style due to the resulting variation in mechanical stratigraphy (Fosdick et al., 2011; Ghiglione et al., 2009; Giacosa et al., 2012; Kraemer, 2003; Kraemer et al., 2002). Although it has been proposed that conspicuous lateral changes in the geometry and distribution of structures from the Patagonian

* Corresponding author at: Laboratorio de Modelado Geológico (LaMoGe), Instituto de Estudios Andinos Don Pablo Groeber, Universidad de Buenos Aires, Ciudad Universitaria, C1428EHA, Buenos Aires, Argentina. Tel.: +54 11 4576 3300/9 int. 287.
E-mail address: jlikerman@gl.fcen.uba.ar (J. Likerman).

0040-1951/$ – see front matter © 2013 Elsevier B.V. All rights reserved.
http://dx.doi.org/10.1016/j.tecto.2013.01.018

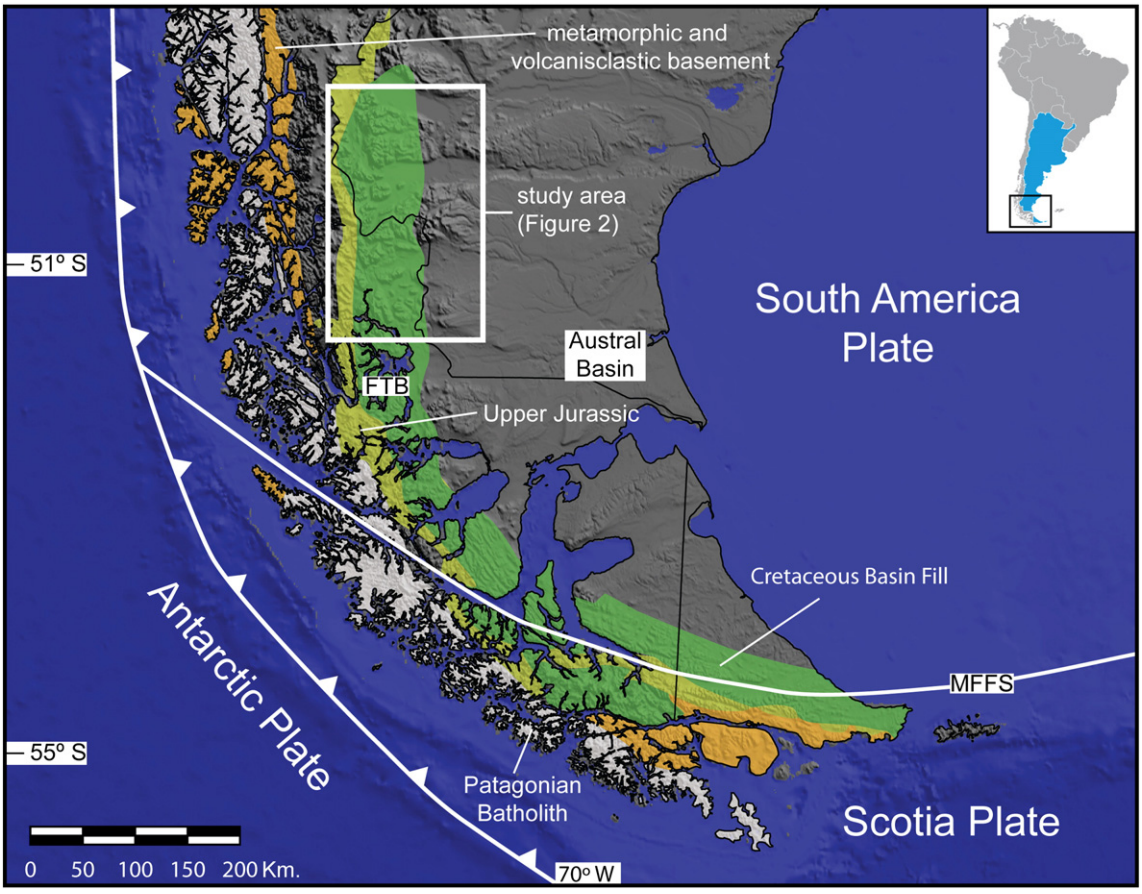

Fig. 1. High-resolution digital elevation model (Mercator projection) from processed National Aeronautics and Space Administration (NASA) Shuttle Radar Topography Mission data (SRTM; Farr et al., 2007) of the southernmost Andes (~38°–56°S). Superimposed on the map are the main morphostructural units of southernmost Patagonia and Tierra del Fuego. Location of study area is highlighted. Abbreviations are: FTB, fold-thrust belt; MFFS, Magallanes-Fagnano fault system.
Adapted from Romans et al. (2010) and Ghiglione et al. (2010).

fold-thrust belt (Fig. 2) are mainly controlled by the position of ancient Jurassic-rift transfer faults (Ghiglione et al., 2009; Giacosa et al., 2012; Kraemer, 1994), there has so far been no comprehensive structural study dedicated to the analysis of this issue.

The purpose of this paper is to test whether the along strike variations seen in the Southern Patagonian Andes, previously described by other authors (Arbe, 1989; Ghiglione et al., 2009; Kraemer, 1994; Kraemer and Riccardi, 1997), are the result of ancient Jurassic-rift transfer faults. With this objective in mind, we designed a set of experiments to simulate the development of an asymmetric rift system in the sense of Serra and Nelson (1988), i.e. a rift composed of depocenters undergoing differential extension.

2. Regional setting and mechanical stratigraphy

The metamorphic basement of the Southern Patagonian Andes, outcropping along the pacific archipelago (Fig. 1), is mainly composed of low-grade metasedimentary rocks interpreted as Late Paleozoic subduction complexes intruded by Mesozoic–Cenozoic granitoids of the Patagonian Batholith (Hervé, 1988). Initial extensional subsidence began in almost all of the Patagonian basins during the Triassic–Jurassic continental rifting of southern South America (Pankhurst, 2000; Uliana et al., 1989).

A middle to late Jurassic extensional phase produced several N–S oriented depocenters controlled by normal faulting affecting the late Paleozoic basement (Biddle et al., 1986; Diraison et al., 2000). The silicic pyroclastic rocks of the Tobífera or El Quemado Formation constituted the synrift sedimentation in N–S grabens within the Paleozoic metasediments (Fig. 3). Stretching was maximum along the Pacific margin and produced oceanic crust in the Rocas Verdes Basin during Middle to Late Jurassic times (Dalziel, 1981). Mechanical subsidence and stretching attenuated towards the eastern craton, as shown by the presence of shallower sequences that are dominated by continental to hemipelagic sequences (Arbe, 1989; Manassero, 1988). The synrift sequences are overlaid by lower Cretaceous sag deposits of the arenaceous Springhill and pelitic Zapata-Río Mayer formations (Fig. 3).

Since the late Cretaceous, compressive deformation propagated eastward, generating at least four orogenic sedimentary sequences (Arbe, 1989; Coutand et al., 1999; Ghiglione and Ramos, 2005; Kraemer, 2003). The coarser proximal facies of these sequences, probably representing pulses of accelerated uplift and propagation of the deformational front, are now involved in the fold-thrust belt, where they are separated by paraconformities or angular unconformities that represent long hiatuses (Fig. 3). Their foreland-distal equivalents, consisting of medium to fine grain sediments, are separated by paraconformities with shorter hiatuses. Some of these units represent Upper Cretaceous to Paleocene hydrocarbon reservoirs (Cagnolatti and Miller, 2002; Limeres and Dellape, 2005; Marinelli, 1998; Zilli et al., 2002). The structural packages involved in compressional deformation are mainly Late Cretaceous to Paleogene sequences associated with tectonic uplift (Fig. 3).

3. Experimental procedure

3.1. Modeling strategy

Scaled analog models are powerful tools for the visualization of the progressive evolution of rift fault systems (McClay, 1990, 1995;

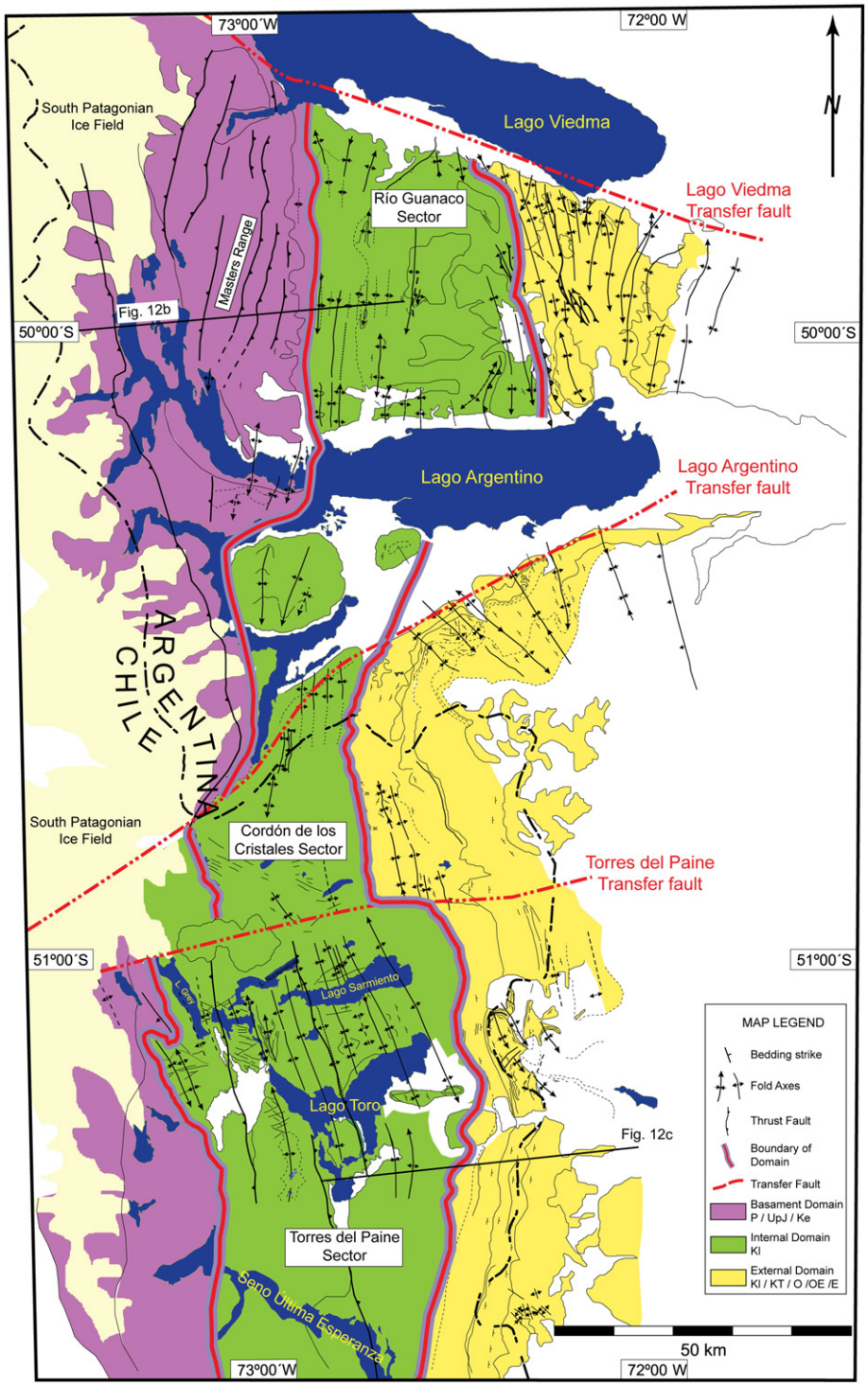

Fig. 2. Structural map of the of the Southern Patagonian Andes, showing structural domains along-strike variations in width and lateral position; and Lago Viedman, Lago Argentino and Torres del Paine Transfer faults. Abbreviations are: P, Paleozoic; UpJ, Upper Jurassic, Ke, Early Cretaceous; Kl, Late Cretaceous; KT, Cretaceous–Triassic; O, Oligocene; OE, Oligocene–Eocene; E, Eocene.
Modified from Ghiglione et al. (2009).

Yagupsky et al., 2008). A number of analog modeling studies have investigated the effect of rift basin development followed by contractional deformation (Amilibia et al., 2005; Brun and Nalpas, 1996; Buchanan and McClay, 1991, 1992; Dubois, 2002; Eisenstadt and Withjack, 1995; Koopman et al., 1987; McClay, 1989; Mitra and Islam, 1994; Panien et al., 2005). In particular Del Ventisette et al. (2005, 2006), Gartrell et al. (2005) and Konstantinovskaya et al. (2007) have explored the role of fault reactivation associated with oblique shortening.

In this work, analog modeling was performed to investigate in detail how differential extension, delimited by a transfer fault, could affect the deformation pattern during basin inversion in the simplest conditions. In the experiments, performed at the Laboratorio de Modelado Geológico (LaMoGe), we tried to reproduce the formation

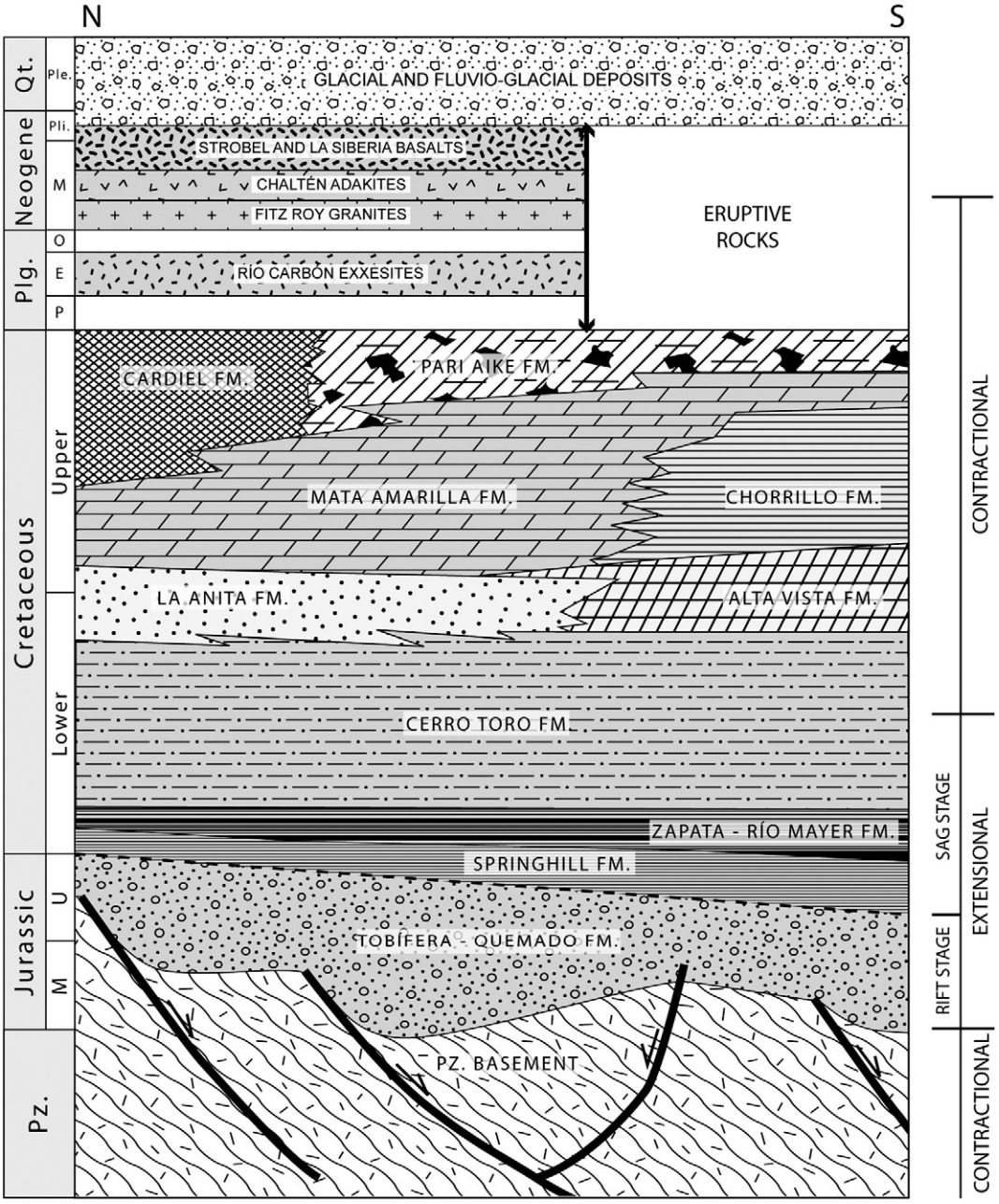

Fig. 3. Generalized tectono-stratigraphic chart for the Southern Patagonian Andes between Lago Argentino and Lago Toro. Based on Arbe (2002), Kraemer and Riccardi (1997), Kraemer et al. (2002) and modified from Giacosa et al. (2012).

of transfer systems in brittle–ductile extensional domains, focusing on those interacting structures that characterize the continuity and shape of rift zones, similar to those observed in the Southern Patagonian Andes. In the experiments we varied the amount of differential extension between adjacent crustal blocks to examine how this parameter affects the generation of a transfer zone and how this structure interact during shortening (Table 1). It is important to note that this work does not take into account pre-rift brittle structures that may appear in nature, even though these may play an important role in the interaction and development of extensional structures (Faccenna et al., 1995; Huyghe and Mugnier, 1992; Ranalli, 2000; Sibson, 1985).

Table 1
Geometric characteristics of the performed analog models. D, initial distance between the two model halves; DE, amount of differential extension between the two model halves (see Fig. 13).

	D (cm)	L_u (cm)	L_l (cm)	DE (%)
MOD_1	8.5	51.5	60	60
MOD_2	6	54	60	40
MOD_3	5	55	60	35

3.2. Experimental set-up

Three models were performed, consisting of two separated steps: the first step generated a rift setting to simulate the interaction between adjacent crustal blocks experiencing different extensional rates accommodated by a transfer fault. During the second step the resulting model from the first step underwent compression forcing the inversion of the system. Model 3 was chosen for detailed description in the following section, and its first step was repeated twice to allow the dissection and scanning of cross sections. The experiments were performed in a non-boundaries deformation rig with dimensions 54×70×4 cm

(Fig. 4), wide enough to achieve a relatively large amount of extension and shortening without border effects. The experimental apparatus consisted of a fixed rigid basal plate over which two acetate sheets attached to the moving walls were pulled by two step-motors driven worm screws. The extensional stage was achieved by pulling the basal acetate sheets in the same direction but at different speeds. One moved with a constant displacement rate of 3.3×10^{-3} cm s^{-1} and the other at 2.3×10^{-3} cm s^{-1}, creating a basal and lateral velocity discontinuity (Fig. 4a). Varying the initial separation between the two moving walls allowed controlling the amount of differential extension between adjacent crustal blocks. When extension ended the two moving walls were aligned in the same position. Accommodation space generated by extension was filled up with blue colored sand replicating synrift sedimentation. Then, a 1-cm thick post-rift brown colored sand package was added over the model.

In the second phase lateral shortening was applied pushing a moving wall in the opposite direction to the extension, at a constant displacement rate of 2.4×10^{-3} cm s^{-1} until a final shortening of 8 cm was achieved (Fig. 4b). A fixed high-resolution digital camera was used to photograph the top surface of the models at regular time intervals in order to study the time–space evolution of the structures. At the end of the experiments, dry sand was sieved on the models surface to preserve the final topography. In order to reconstruct a three-dimensional geometry, the models were impregnated with hot gelatin solution and, once cooled slightly hardened, were sliced (~5 mm) perpendicular to the structures strikes. In this way internal structural arrangements of the final state of the models could be analyzed.

The top surfaces of the models were scanned with a laser (~0.135 mm of accuracy) at regular time intervals. The data obtained were processed to remove spurious data. Subsidence of the top surface was calculated from the incremental difference between successive gridded data. In the shortening phase, incremental topographic maps were obtained, revealing the development of contractional structures. This methodology used along with photography allows a more rigorous and detailed interpretation of the development of the structures.

3.3. Model materials

Brittle layers are represented by well sorted dry quartz sand with well-rounded grains, smaller than 500 μm and density (ρ) around 1400 kg/m^3. In material such as this, frictional contacts between the grains result in a failure envelope of Mohr–Coulomb type with small cohesion (<100 Pa) and an angle of internal friction close to 32.7° (Yagupsky et al., 2008), measured with a modified Hubber-type shear apparatus (Hubbert, 1951). The prekinematic pile, composed of black and white sand, was mechanically sieved over the modeling rig in order to get homogeneous layers with an average thickness of 0.5 cm.

The stretching at the base of the brittle upper crust was modeled with a clear, viscous fluid, which is formed by the cross-linking of polyvinyl alcohol with a boron compound (Casassa et al., 1986; Stewart, 1996). This material flows under low stress and has the property of breaking under higher stresses and pressures, because of this behavior it can be considered a Maxwell solid (Casassa et al., 1986) with a viscosity in the order of 2.5×10^3 Pa s (Stewart, 1996). The use of a 0.5 cm thick layer of this material on top of the basal velocity discontinuity (BVD) had the purpose of controlling the location of the fault nucleation, and consequently the configuration, i.e. orientation, length, overlap length and spacing of the overstepping normal faults. In these experiments the ductile material does not simulate any character of the crust and has an exclusively geometrical use (Brun and Nalpas, 1996).

3.4. Model scaling

In order to compare analog models with natural examples, the experiments should be geometrically, kinematically and dynamically scaled (Hubbert, 1937; Ramberg, 1981). In the experiments carried out, the length ratio between model and nature is $L=10^{-5}$ (1 cm

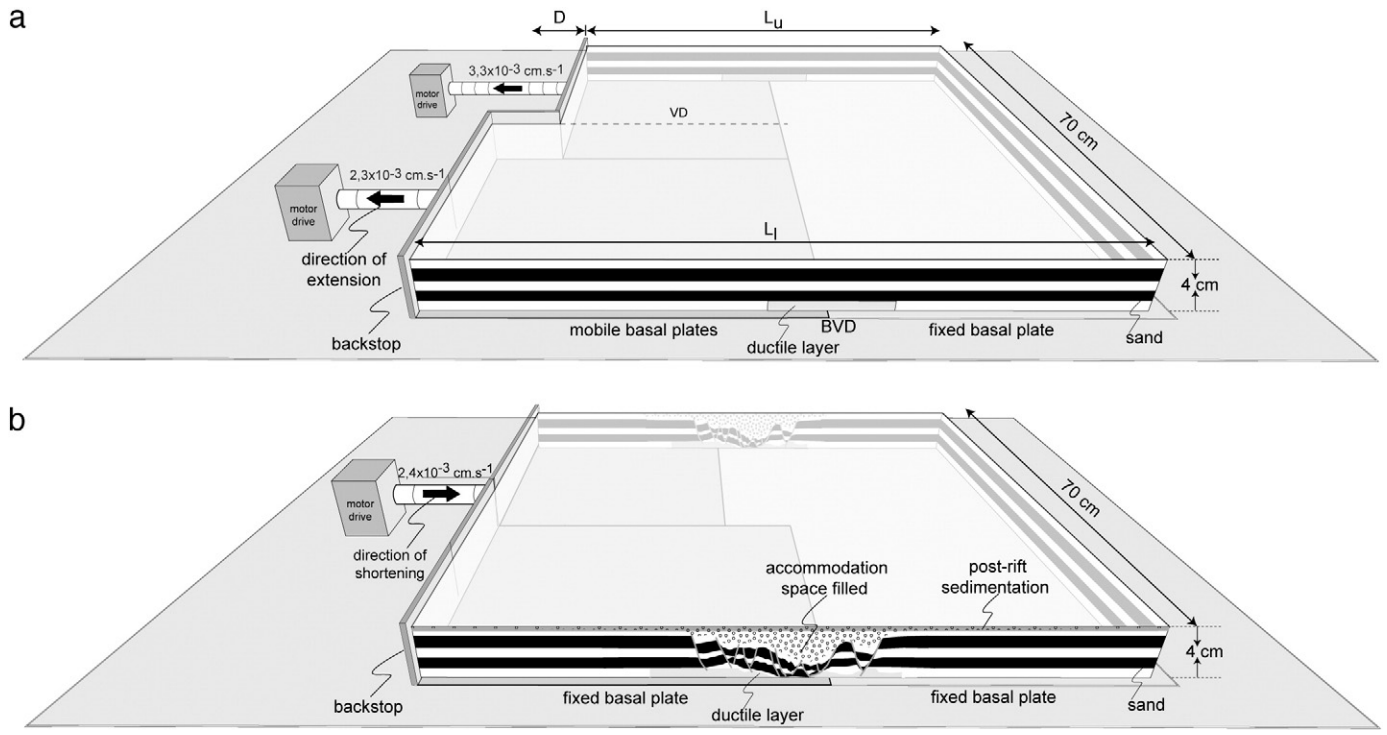

Fig. 4. Experimental apparatus. a) Sketch of model set-up, assembly and initial dimensions for all models. VD indicates the lateral velocity discontinuity between de mobile basal plates; BVD stands for basal velocity discontinuity at the base of the model. b) Experimental apparatus and model setting for the shortening phase. The basal acetate sheets are disconnected from the moving wall to minimize their role during the inversion phase. See D values in Table 1.

Table 2
Scaling parameters and ratios for nature and models.

	λ (m)	g (m/s^2)	ρ (kg/m^3)	μ (Pa s)	V (m/s)	σ (Pa)	ε (s^{-1})
Nature	1000	9.81	2300	2×10^{20}	5×10^{-12}	2.2×10^{7}	10^{-14}
Model	0.01	9.81	1400	2.5×10^{3}	2.4×10^{-5}	1.4×10^{2}	4.8×10^{-3}
Model/nature(*)	10^{-5}	1	0.6	1.25×10^{-17}	$4{,}8\times10^{6}$	6×10^{-6}	4.8×10^{11}

in the model correspond, approximately, 1 km in nature); the density ratio between common experimental granular materials and rock is $\rho\approx0.6$; and the gravity ratio between model and nature is $g^*=1$, as both the prototype and the model are subject to the same value of gravitational acceleration. The corresponding stress ratio between model and nature is $\sigma^*=\rho^*\,g^*\,\lambda^*\approx6\times10^{-6}$.

For Newtonian ductile materials, the following relation applies (Benes and Davy, 1996):

$$\sigma^* = \mu^*\varepsilon^* \quad (1)$$

where μ^* and ε^* are the viscosity and strain rate ratios between the model and nature, respectively. Considering natural strain rates in rocks (ε_n) vary between 10^{-15} and 10^{-13} s^{-1} (Pfiffner and Ramsay, 1982) and assuming an average natural strain rate of 10^{-14} s^{-1}, $\varepsilon^*=4.8\times10^{11}$ (Table 2). From Eq. (1), follows that $\mu^*=1.25\times10^{-17}$ implying that the model viscosity ($\mu_m=2.5\times10^{3}$ Pa s) corresponds to a natural viscosity of 2×10^{20} Pa s, which is sufficiently similar to those commonly used for high décollement viscosities (Weijermars, 1993). The models are thus broadly scaled to represent a strong natural décollement. As $V^*=\varepsilon^*/L^*$, $V_n=5\times10^{-12}$ m s^{-1}, this value corresponds to a natural velocity of 0.16 mm/year, which is comparable with slow natural rates of thrusting (Table 2).

4. Model results

4.1. Extensional phase (Model 3)

4.1.1. Plan view evolution

The structural configuration obtained was relatively similar in all three experiments. Between each experiment the variable parameter was the amount of extension between the two blocks separated by a transfer fault. Modeling results of experiment MOD_3 are

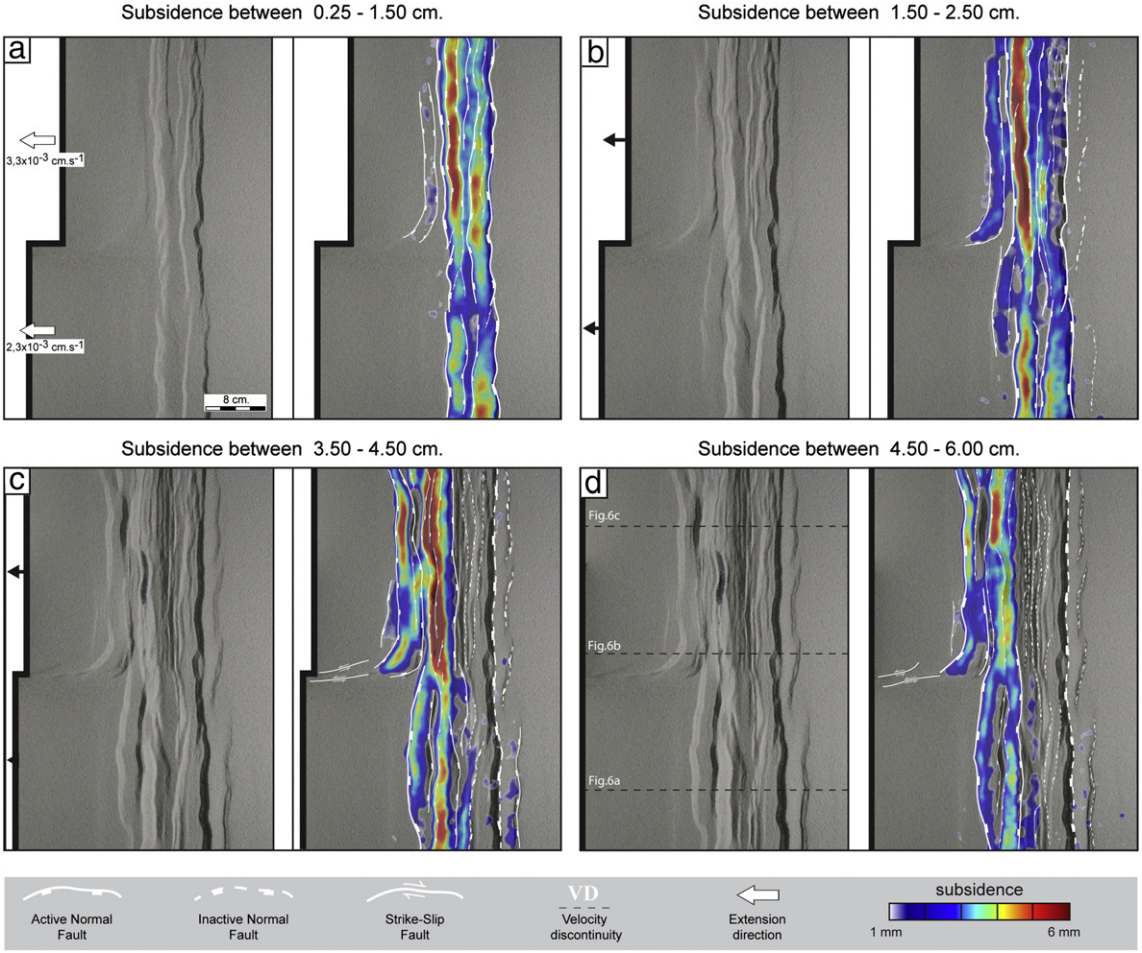

Fig. 5. Plan view evolution of extensional model (MOD_03) for four displacement stages, without synrift sedimentation. Photographs show top-view of the surface of the model. The fault pattern interpretation and incremental basin subsidence calculated from differential laser scans are shown at each step of the progressive extension. Lateral velocity discontinuity (VD) in dashed line. Arrows indicate extension direction and velocity. The dashed black lines in d indicate the trace of the cross sections shown in Fig. 6.

summarized in Fig. 5. Sequential photographs of top of the 3D models during the experiment evolution, together with fault interpretation and subsidence isopach maps highlighting the differential subsidence between each stage are presented. Additionally internal structure interpretation is shown in serial vertical sections for the end of this phase. With a descriptive purpose, we will use the terms proximal and distal according to their proximity to the advancing moving wall, forethrusts for those faults dipping toward the moving wall and backthrusts for those dipping in the opposite direction.

Initial phases of extensional deformation (0.25 to 1.50 cm extensional displacement) resulted in soft rift-borders parallel to the moving backstops, well defined in the upper half of the model (above the lateral velocity discontinuity) and just incipient in the lower half. The isopach map highlights the differential subsidence between the non-deformation stage and the 1.50 cm of extensional displacement. Between this phase well developed straight rift-borders are established (Fig. 5a). A central horst, limited by minor extensional faults with opposite dip directions, constitutes a topographic high formed in the sector of minimum stretching. In the upper half the horst appears segmented by a larger number of minor faults.

From 1.50 to 2.50 cm of extensional displacement, straight borders started to lose sharpness. The topographic highs, begin to be dissected by small internal faults, while in the lower half, this feature is still well expressed. Subsidence maps show that extension is concentrated in a continuous central graben, parallel to the moving wall. The extensional system above the slower plate starts to widen through graben propagation to the backstop. The lateral termination of graben features along the VD is marked by relay ramps or accommodation zones, characterized by normal faults that became, slightly oblique to the extension direction (Fig. 5b).

After 4.5 cm of displacement, the deformation focus migrates towards the backstop, leaving earlier distal normal faults inactive

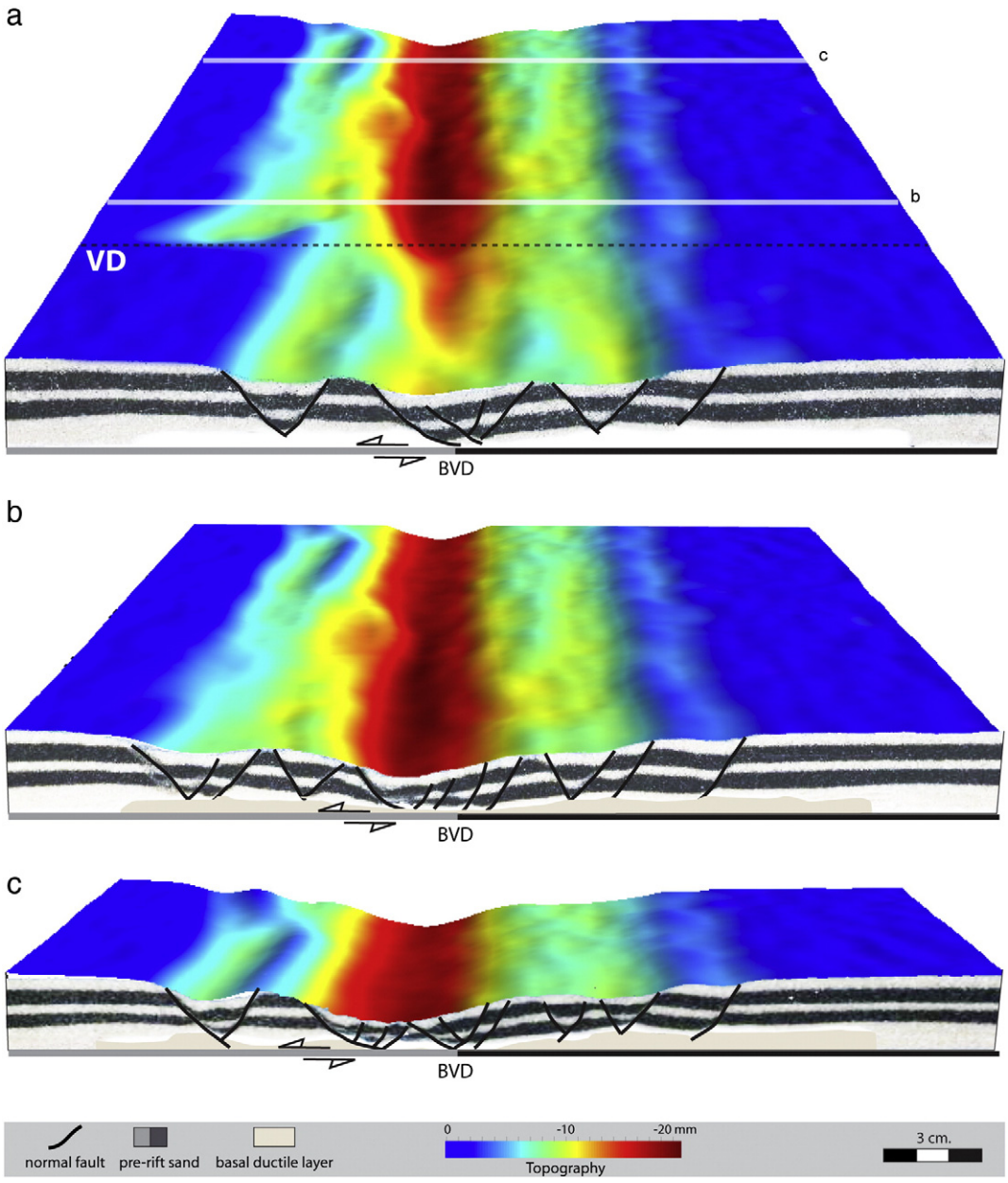

Fig. 6. 3D block visualization of the final topography and fault pattern interpretation of serial sections at the end of extension, without synrift sedimentation. Pre-kinematic strata are black and white layers whereas the ductile material is the gray layer. The location of the cross-sections is shown in Fig. 5d. VD: lateral velocity discontinuity; BVD: basal velocity discontinuity.

(Fig. 5c). However, this process is stronger in the upper half than in the lower half, where some distal faults are still active. The lateral termination of these graben-like features along the VD occurs by means of transfer faults, while away from the VD the type of interaction continue through relay ramps, meaning areas of reoriented bedding between normal faults that overstep in map view (Peacock et al., 2000). An important process at this stage is the generation of incipient strike-slip movements along the coupling zone between baseplates. It is remarkable, that while in the upper half the axis of the outer subbasin bend parallel to the extension direction near de the VD, the corresponding subbasin in the lower half, does not show this feature and its margins develop parallel to the backstop walls without showing any interaction with the VD (Fig. 5c). The extension ended at 6.00 cm of displacement, this last stage emphasizes the development of normal faulting in the upper half sector. Normal faults grow closely spaced ending laterally against the central strike-slip zone, the rift border faults and the intra-rift faults systems break almost 45° when they reach the VD (Fig. 5d).

4.1.2. Vertical sections

Vertical serial cross sections were used to reconstruct the internal geometry of the model at the final stage. Fig. 6 shows three sections of the model produced to illustrate the structure in the upper and lower half and the transfer zone on the VD. Section A has a complex array of faults with a central graben delimiting the deepest zone. The angles of inclination of the faults are 55°–40°. Symmetrically on either side of the central graben, two horst comprise the inside basin highs, which are bounded externally by two grabens, whose outer limits mark the basin borders (Fig. 6a).

Section B, located near the VD, shows normal faults with dip angles between 60°–45° and dominant left-dipping domino fault arrays with few antithetic faults defining lower areas of the model. The graben formed in the strike-slip zone is delimited by a horst to the right and concave-up fault to the left (Fig. 6b). The section in the upper half (Section C) shows an array of normal faults, with dip angles between 55°–40°. The deepest part of the basin has a more complex arrangement, listric normal faults, with angles from about 40° near the surface which decrease to 20° in the ductile decollement layer at depth. Associated with these listric faults, small antithetic normal faults are laying against the fault plane (Fig. 6c).

4.2. Shortening phase (Model 3)

4.2.1. Plan view evolution

Modeling results of experiment MOD_03 are summarized in Fig. 7. Isopach maps highlighting the differential uplift between each stage are presented. The initial shortening stage (1.00–2.50 cm, Fig. 7a) produces two proximal forethrusts and splays parallel to the compressional moving wall. Their strike changes abruptly when reaching the VD, revealing a first order controlling feature at the beginning of the experiment. A backthrust develops following the pre-existing rift border fault, and also shows an inflection-bending strike turn

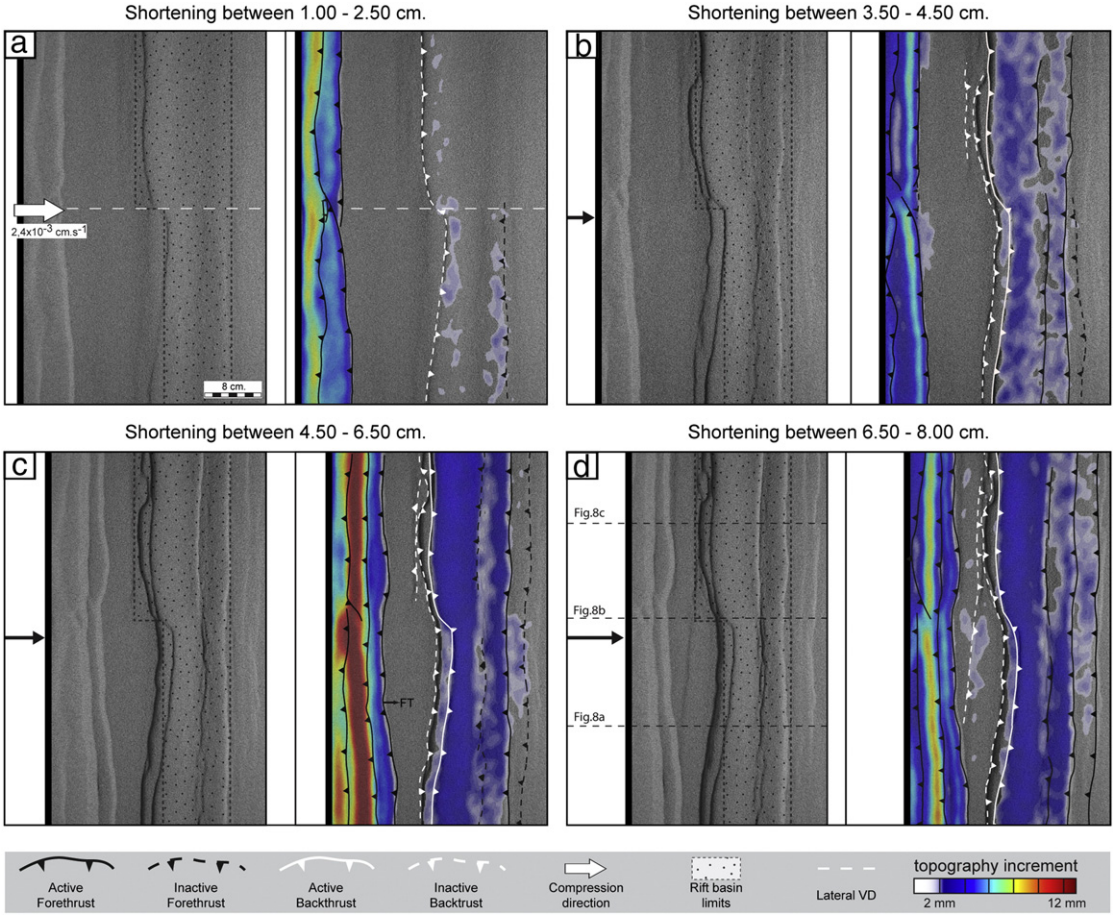

Fig. 7. Plan view evolution of compressional model (MOD_03) for four shortening stages. Photographs show top-view of the surface of the model. The fault pattern interpretation and incremental topographic map calculated from differential laser scans is shown at each step of the progressive shortening. Dashed white line in a indicate the position of VD during extension. The dotted box marks the rift-segments position. Arrows indicate extension direction and velocity. The dashed black lines in d indicate the trace of the cross sections shown in Fig. 8. FT: front thrust.

inside the VD zone. At the next stage (3.50–2.50 cm, Fig. 7b), the deformation jumped to the border of the inverted rift, and a new set of distal forethrust parallel to the compressional moving wall was created. The basin inversion is controlled by major inverted faults with opposite vergence directions (see rift basin limits in Fig. 7).

With 6.5 cm of accumulated shortening, both the proximal deformation front thrusts (FT in Fig. 7c) and the distal basin forethrusts and backthrusts show intense activity. The incremental topographic map point out the activity of the deformation wedge, showing that at the same time as a new thrust is created towards the foreland, ancient thrusts are reactivated. The final stage (6.50 to 8.00 cm of shortening) shows the reactivated basin borders and a partial reactivation of internal basin faults. It is noteworthy that the trend of forethrust and backthrusts suffer an abrupt change when they bypass through the transfer zone formed during the extensional stage, being forced to change their strike direction associated with this feature (Fig. 7d).

4.2.2. Vertical sections

The internal structure of the compressional model is shown by three interpreted cross-sections, one along the VD, and the others in the upper and lower half of the model (Fig. 8). The syn-rift sand thickness was used to identify inverted faults. Syn-rift sand deposited in the hangingwall of normal faults are thicker than the equivalent

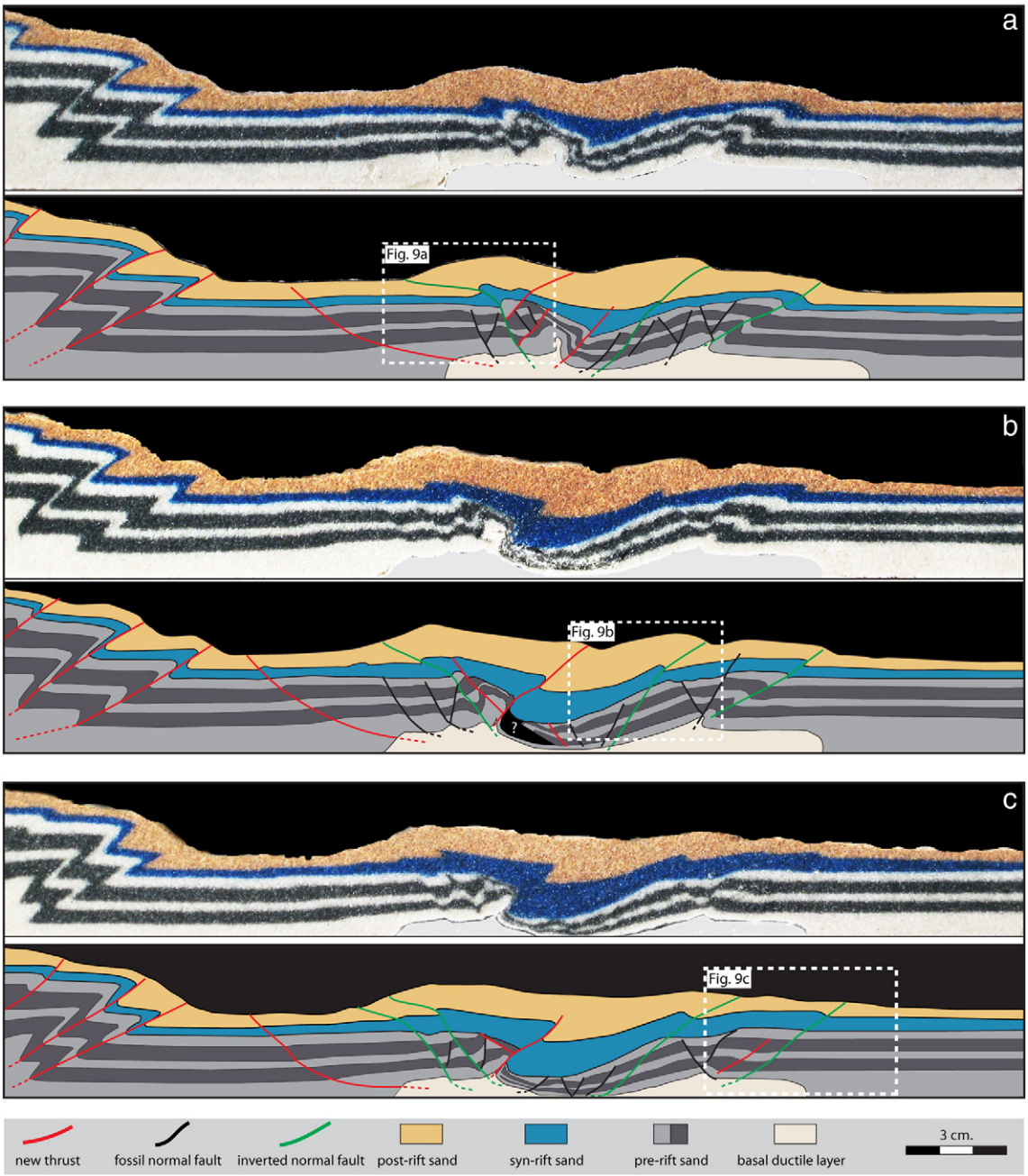

Fig. 8. Cross-sections photographs and fault pattern interpretation of serial sections, cut parallel to the compression direction. The location of the cross-sections is shown in Fig. 7d. Pre-kinematic strata are black and white layers, whereas the ductile material is the gray layer. Accommodation space generated by extension was filled with blue layer sand and post-rift brown colored sand was added over the models before compression.

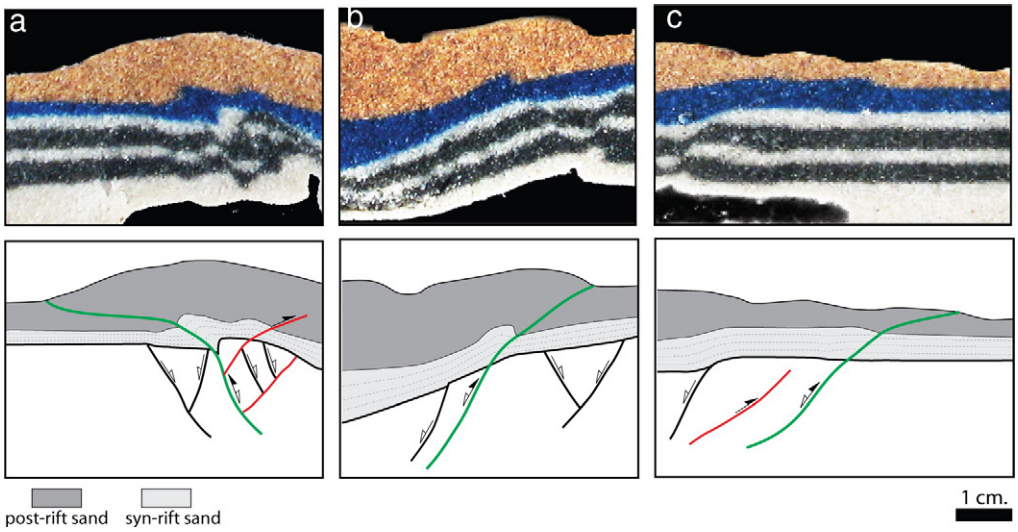

Fig. 9. (a–c) Close ups of cross section shown in Fig. 8. These show deformation styles of shortened (inverted) normal faults. These examples show that thicker packages of syn-rift sand is lifted on the hangingwall of positively inverted faults. Green line, inverted normal fault; black line, not-reactivated normal fault; red line, new thrust fault.

footwall; so inversion will show thicker packages of syn-rift lifted on the hangingwall of positively inverted faults (for details see Fig. 9).

Model cross section in the lower half (Fig. 8a) shows a forethrust sequence with angles of approximately 35°–25° detaching from the backstop. More distally the inverted basin is dominated by listric reactivated normal faults. At the center of the section, the reactivated normal faults exposed in the central part of the cross section dip 60°–40° at depth and flattened (20–35°) near to surface. The opposite part of the inverted basin shows inverted normal faults with different amounts of shortening, showing inversion that is beyond total (i.e., 100% inversion), partially inverted faults and 'fossil' normal faults.

The section along the VD (Fig. 8b) shows a similar structural geometry to that described above; with the difference, that the shortening to the right is mostly concentrated at the rift-border; while normal faults remain totally inactive (Fig. 9b). The inversion in the section corresponding to the lower half of the model is concentrated in both extensional basin borders. A pop-up structure is developed with high dip-slip component, one of the faults that delimits this structure is a reactivated backthrust, with the other conjugate new thrust that dips oppositely to the inverted normal fault (Fig. 8c).

5. Discussion

5.1. Implications for the development and inversion of rift basin

The analog models presented here (Fig. 10) have yielded very interesting results that allow the influence of pre-existing structures derived from an asymmetric rift (i.e. composed of adjacent depocenters experiencing different extensional rates accommodated by a transfer fault). The presented results also show close affinities with the results of previous works analyzing the inversion of symmetric rift-basins (Acocella et al., 2005; Bonini et al., 2012; Del Ventisette et al., 2006; Panien et al., 2006) and works dealing with transfer zones and fault reactivation in inverted rift basins (e.g. Eisenstadt and Withjack, 1995; Gartrell et al., 2005; Konstantinovskaya et al., 2007). During extension, the experiments show that minor differential displacements between adjacent extensional structures are accommodated by relay ramps. This is well represented in the early stages of the extensional model. During extension, the experiments show that minor differential displacements between adjacent extensional structures are accommodated by relay ramps (Fig. 5b) well developed and linked up with adjacent structures. While with further extensional displacement, large displacements can be only accommodated by transfer faults parallel to the extension direction (Fig. 5d).

The plan view evolution and cross sections of the shortening phase show that deformation is focused along pre-existing structures (Fig. 9), favorably at rift borders. With the exception of the newly-formed thrusts developed next to the moving wall and some small faults inside the rift. Reactivated normal faults in our experiments rotated and flattened during shortening (Fig. 9) similar to the analog experiments of Konstantinovskaya et al. (2007) but different from the models of Gartrell et al. (2005) were rift faults locked up followed by cut-off thrust development. During shortening, rift margins underwent reverse displacement with initial high dip angles along the pre-rift layers (50–60°); however when these faults cut the syn-rift and post-rift layers, reactivated normal faults rotated to low-angle faults (20–35°). These results are partially similar to Konstantinovskaya et al. (2007), in which reactivated normal faults rotated to become progressively flatter with continued shortening.

The final deformational pattern is characterized by reverse faults typically developed perpendicular to the shortening direction. Evidence of reactivated transfer faults is observed in the top-view photographs during the first stages of shortening (Fig. 10). Inverted normal faults change their orientation nearly 30° in the direction of compression near the transfer fault zones. Moreover, newly-formed thrusts generated near the moving wall also show evidence of being controlled by orthogonal pre-existing transfer faults (Fig. 10). The traces of the thrust faults are continuous up to the pre-existing transfer zone, where they lose continuity, change strike direction or are terminated.

Transfer zones developed in the three models during extension exert significant control over the structures during the shortening phase. This control is better expressed in models with greater differential extension, characterized by faults ending against the transfer zone (Fig. 10). These results are similar to those described in top-view from the models of Konstantinovskaya et al. (2007), in which deviation of folds and thrusts was observed above the transfer zone. It is conceivable that at greater amount of differential extension between adjacent crustal blocks, normal faults developed in this phase lose along-strike continuity and, during shortening, these structures are reactivated without along-strike propagation and linkage.

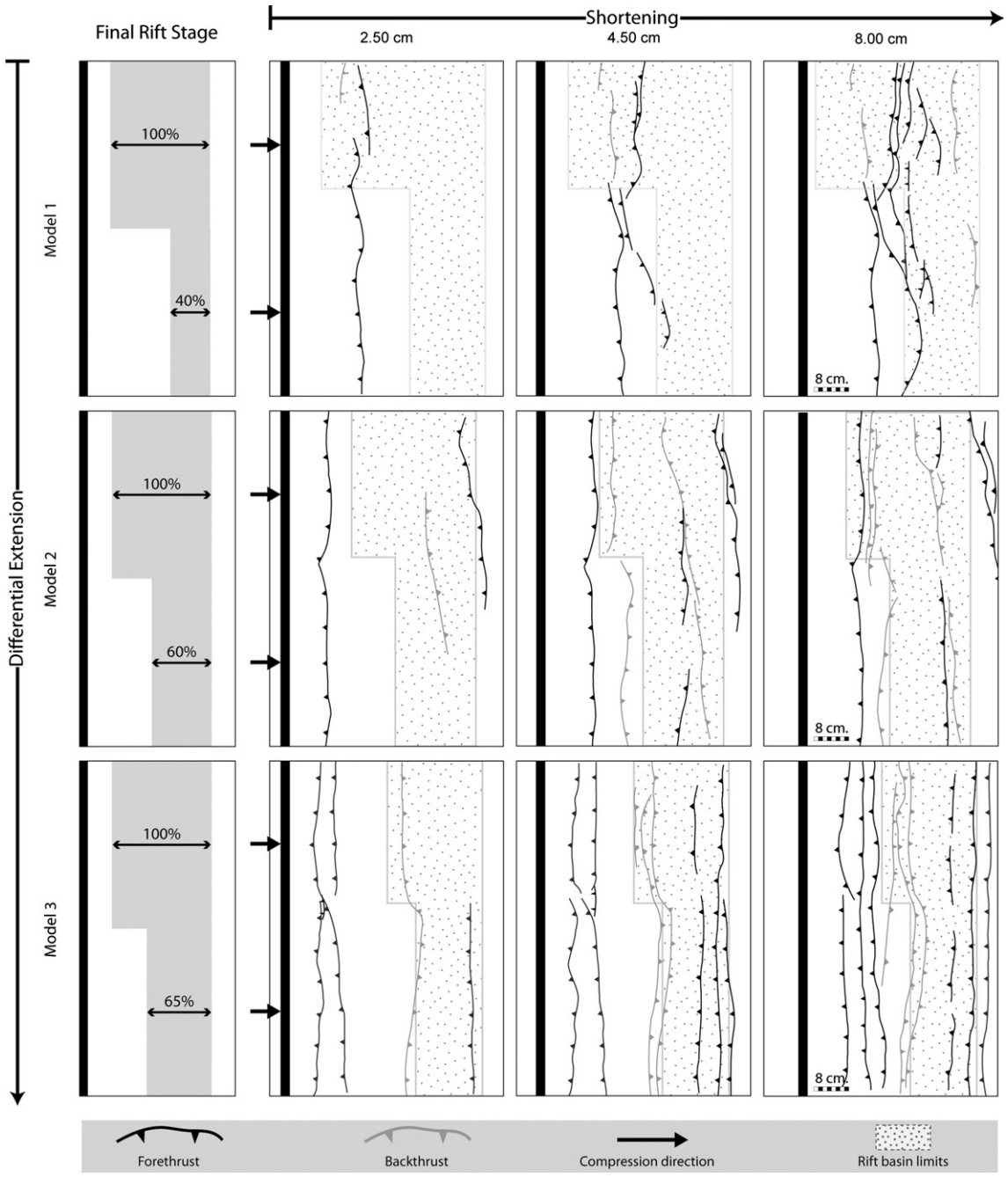

Fig. 10. Line drawings of top view of all models at different shortenings. The relationship between the amounts of extension between the two rift segments increases along the Y axes, while the shortening applied increases along the X axes.

5.2. Correlation between structures in Southern Patagonian Andes and features from the model

The fold-thrust belt from Austral and neighboring foreland basins of southern South America (Fig. 1) are commonly affected by rift inversion (see Ghiglione et al., 2010 for a review). Furthermore, it has been recently demonstrated that the Patagonian Jurassic transfer faults were prone to reactivation under small amounts of stretching orthogonal to their orientation, developing the eastern Magellan strait (Ghiglione et al., 2013). In this context, it has been proposed that strong along-strike variations in width and lateral position of the structural domains that characterize the Southern Patagonian Andes are mainly controlled by the reactivation of ancient Jurassic-rift transfer faults (Ghiglione et al., 2009; Giacosa et al., 2012; Kraemer, 1994). From this conceptual understanding, it has been suggested that adjacent extensional depocenters with different widths reflecting variable degrees of extension would produce this map view geometry during tectonic inversion, without involving significant strike-slip displacement (Ghiglione et al., 2009).

Our analog modeling was designed to test this hypothesis, creating a rift that reconstructs an asymmetric extensional stage with two rift-segments with different behavior separated by a transfer zone.

The transition zones limiting the Río Guanaco, Cordón de los Cristales and Torres del Paine sectors (Fig. 2) are located where large variations in width of the structural domains take place during the shortening phase. Stratigraphic data point out a first-order increase in the fill-thickness and depth to the basement from north to south

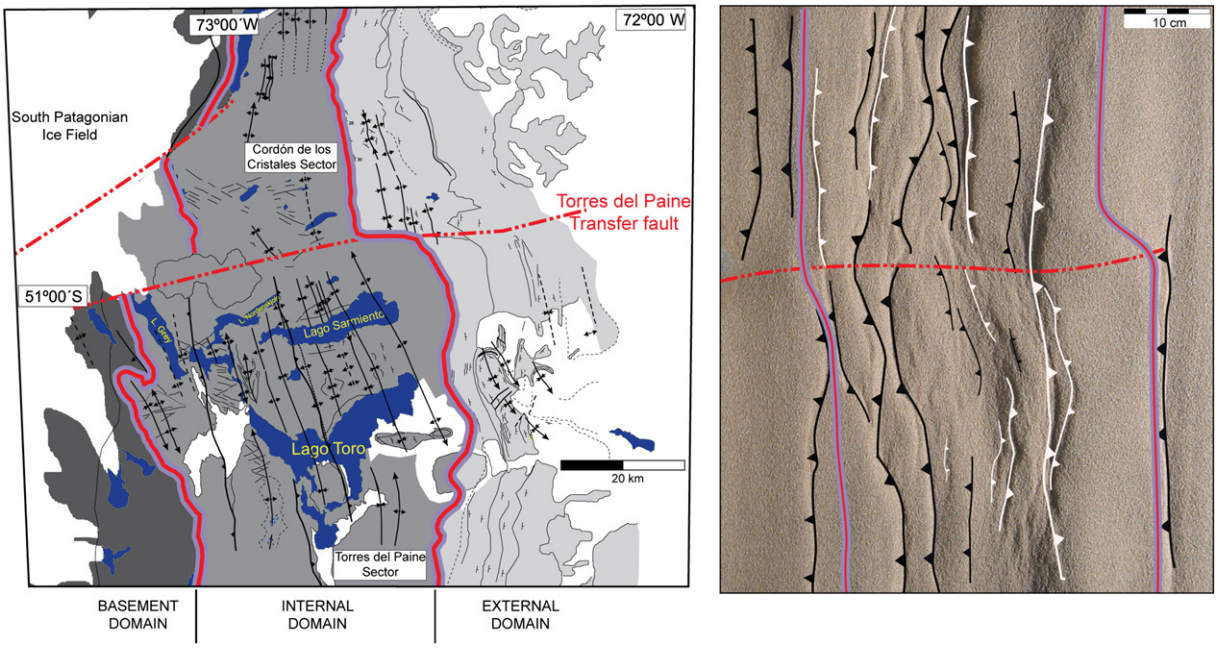

Fig. 11. Comparison of the natural example in the Cordon de los Cristales and Torres del Paine sector from the Southern Patagonian Andes and fault pattern interpretation of the final stage of Model 1. Note the roughly similar domain boundary shape in nature and in the model. Symbols and keys are as those in Figs. 2 and 7. See Fig. 2 for location.

in this sector (Macellari et al., 1989; Manassero, 1988; Romans et al., 2009; Shultz et al., 2005), reflecting a north to south increase in Jurassic stretching that had a major influence on paleobathymetry and subsequent sedimentation (Romans et al., 2009). The model geometries can then be compared with the transition zones limiting the above mentioned sectors of the Southern Patagonian Andes, where reactivation and inversion of pre-existing extensional faults in the dominant way of absorbing the shortening and also, where the structural domains are controlled by the position of ancient Jurassic-rift transfer faults (Fig. 11). Well-developed inversion structures with similar characteristics to those formed in the experiments have also been documented in the Patagonian retroarc fold and thrust belt (e.g. Fosdick et al., 2011). In contrast, the thrust folds and fault traces developed in the experiments do not seem to stop at the transfer zone as observed in the natural example, but deviations in the structural strike of fold axes and fault traces within the transfer zone are the dominant style. However it is possible to observe a significant kinematic and geometric asymmetry between inverted rift segments occurred during the progress of the experiments (Fig. 7). Structural variations between these two sectors are seen abruptly from either side of the transfer zone, allowing the delimitation of structural domains similar to those observed for the natural example.

In the Rio Guanaco sector a regional balanced cross section from Kraemer (1998) between Lago Viedma and Lago Argentino (Fig. 12) shows remarkable similarities with the sections obtained from our models. Both model and nature display west-vergent thrust systems delimiting the Basement Domain (BD) and the Internal Domain (ID). In both cases a backthrust develops just next to this thrust system, and between these two systems, there is a sector with subhorizontal strata (Fig. 12b). Additionally, regional two-dimensional seismic-reflection data from Fosdick et al. (2011) of the Patagonian thrust belt and Magallanes retroforeland basin located on the Torres del Paine sector, allows a qualitative comparison between the faults arrangement in the subsurface (Fig. 12c). These authors interpreted a deep detachment level within the Paleozoic basement associated with the thick-skinned thrust system. In particular the Toro thrust located west of the external domain, accounts for uplift and folding of Paleozoic basement, overlying the synrift deposits, and Upper Cretaceous foreland strata. These geometries can be also compared with the inverted thrust of the vertical section shown Fig. 12a, that is associated with the basal detachment and that deformed the syn-rift and foreland basin fill. Moreover, both model and nature display very similar fault architecture, these being characterized by the presence of fossil normal faults over the inverted fault. In the case of Fosdick et al. (2011) interpretation, the normal fault have evidence of reactivation and they do not interpret the thrust as a reactivated normal fault, this is different from our models.

6. Conclusions

Analog modeling techniques were used to investigate the along-strike variations in the Southern Patagonian Andes. Analog models permitted a clear observation of the effects of transfer faults on the structural evolution and architecture of an inverted basin interpreted to resemble parts of the Austral or Magallanes basin. During extension, transfer zones developed and accommodated the offset between rift segments. A strong variation in width and lateral position of main thrusts during the compressional stage of the model occurred near the transfer zone. Deviation of fold axes and deflection of thrust and backthrust in sand layers were observed within transfer zone during shortening, in agreement with the idea that similar variations found in the Patagonian fold-thrust belt coincide with ancient transfers zones between the rift segments, possibly due to the development of an asymmetric rift.

Broad comparison between the structural architecture of the experimental models can be made with that of Rio Guanaco, Cordon de los Cristales and Torres del Paine sectors in the Patagonian Andes. The inversion of extensional structures produces a geometry that is consistent with cross-sections from field and seismic data for the proposed study area. Pre-existing normal faults partially inverted during shortening seems to control the localization and geometry of contractional structures.

Analog modeling carried out in this paper allows a clearer picture of the evolution of the Southern Patagonian Andes and provides a better

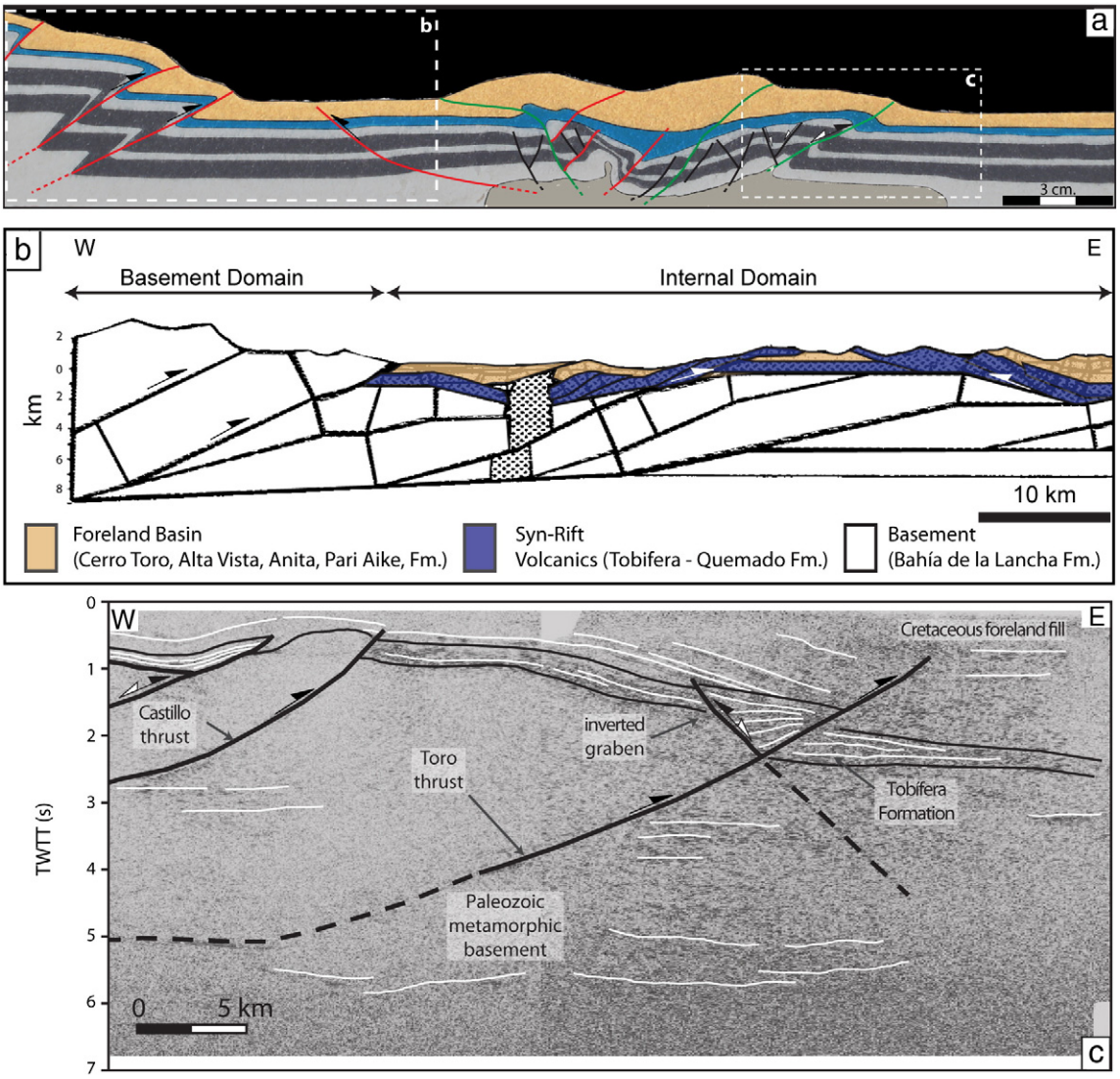

Fig. 12. Comparison of structural cross sections. a) Fault pattern interpretation of model serial section cut parallel to the compression direction (for location see Fig. 8a). b) Regional balanced cross section, see Fig. 2 for location. c) Regional two-dimensional seismic-reflection data and line drawing interpretation across the frontal thrust of the Patagonian fold-and-thrust belt. Refer to Fig. 2 for location of the seismic-reflection line. Symbols and keys are as those in Fig. 8.
b, modified from Kraemer (1998); c, modified from Fosdick et al., 2011.

understanding of the possible causes of differences in the orientation and culminations of structures during basin inversion. Moreover, this final configuration supports the hypothesis of an asymmetric rift history followed by a symmetrical compression.

Acknowledgments

This work has been carried out with the financial support of grants UBACyT X855 and X055, and projects Agencia PICT 2010-00036 and CONICET PIP 0048. This is the contribution R-79 of the Instituto de Estudios Andinos “Don Pablo Groeber” (UBA-CONICET). Special thanks are due to Dr. Marco Bonini for his time dedication and his stimulating and constructive review which helped to improve the manuscript. We also thank Dr. Daniel L. Yagupsky for inspiring discussion and helpful suggestions.

Appendix A. Supplementary data

Supplementary data associated with this article can be found in the online version, at http://dx.doi.org/10.1016/j.tecto.2013.01.018. These data include Google map of the most important areas described in this article.

References

Acocella, V., Morvillo, P., Funiciello, R., 2005. What controls relay ramps and transfer faults within rift zones? Insights from analogue models. Journal of Structural Geology 27, 397–408.
Amilibia, A., McClay, K.R., Sabat, F., Muñoz, J.-A., Roca, E., 2005. Analogue modelling of inverted oblique rift systems. Geologica Acta 3, 251–271.
Arbe, H., 1989. Estratigrafía, discontinuidades y evolución sedimentaria del cretácico en la Cuenca Austral, provincia de Santa Cruz. Cuencas Sedimentarias. Universidad Nacional de Tucumán Serie Correlación Geológica, pp. 419–442.
Arbe, H., 2002. Análisis estratigráfico y facies de depósitos continentales, litorales, y marinos del Cretácico Superior, Lago Argentino, provincia de Santa Cruz. 9° Congreso Geológico Argentino, Actas, 7, pp. 124–158.
Beauchamp, W., 2004. Superposed folding resulting from inversion of a synrift accommodation zone, Atlas Mountains, Morocco. AAPG Special Volumes 82, 635–646.
Benes, V., Davy, P., 1996. Modes of continental lithospheric extension: experimental verification of strain localization processes. Tectonophysics 254, 69–87.
Biddle, K.T., Uliana, M.A., Mitchum, R.M., Fitzgerald, M.G., Wright, R.C., 1986. The stratigraphic and structural evolution of the central and eastern Magallanes basin, southern South America. In: Allen, P.A., Homewood, P. (Eds.), Foreland Basins. Blackwell Publishing Ltd., Oxford, UK, pp. 41–61.

Bonini, M., Sani, F., Antonielli, B., 2012. Basin inversion and contractional reactivation of inherited normal faults: a review based on previous and new experimental models. Tectonophysics 522–523, 55–88.
Brun, J.-P., Nalpas, T., 1996. Graben inversion in nature and experiments. Tectonics 15, 677.
Buchanan, P.G., McClay, K.R., 1991. Sandbox experiments of inverted listric and planar fault systems. Tectonophysics 188, 97–115.
Buchanan, P.G., McClay, K.R., 1992. Experiments on basin inversion above reactivated domino faults. Marine and Petroleum Geology 9, 486–500.
Cagnolatti, M., Miller, M., 2002. Los reservorios de la Formación Magallanes. In: Schiuma, Hinterwimmer, Vergani (Eds.), Rocas Reservorio De Las Cuencas Productivas De La Argentina, pp. 91–117.
Carrera, N., Munoz, J., Sabat, F., Mon, R., Roca, E., 2006. The role of inversion tectonics in the structure of the Cordillera Oriental (NW Argentinean Andes). Journal of Structural Geology 28, 1921–1932.
Casassa, E.Z., Sarquis, A.M., Van Dyke, C.H., 1986. The gelation of polyvinyl alcohol with borax: a novel class participation experiment involving the preparation and properties of a "slime". Journal of Chemical Education 63, 57.
Coutand, I., Diraison, M., Cobbold, P.R., Gapais, D., Rossello, E.A., Miller, M., 1999. Structure and kinematics of a foothills transect, Lago Viedma, southern Andes (49°30′S). Journal of South American Earth Sciences 12, 1–15.
Dalziel, I.W.D., 1981. Back-arc extension in the Southern Andes: a review and critical reappraisal. Philosophical Transactions of the Royal Society A: Mathematical, Physical and Engineering Sciences 300, 319–335.
Del Ventisette, C., Montanari, D., Bonini, M., Sani, F., 2005. Positive fault inversion triggering "intrusive diapirism": an analogue modelling perspective. Terra Nova 17, 478–485.
Del Ventisette, C., Montanari, D., Sani, F., Bonini, M., 2006. Basin inversion and fault reactivation in laboratory experiments. Journal of Structural Geology 28, 2067–2083.
Diraison, M., Cobbold, P.R., Gapais, D., Rossello, E.A., Le Corre, C., 2000. Cenozoic crustal thickening, wrenching and rifting in the foothills of the southernmost Andes. Tectonophysics 316, 91–119.
Dubois, A., 2002. Analogue modelling of fault reactivation: tectonic inversion and oblique remobilisation of grabens. Journal of Structural Geology 24, 1741–1752.
Eisenstadt, G., Withjack, M.O., 1995. Estimating inversion: results from clay models. Geological Society, London, Special Publications 88, 119–136.
Faccenna, C., Nalpas, T., Brun, J., Davy, P., Bosi, V., 1995. The influence of pre-existing thrust faults on normal fault geometry in nature and in experiments. Journal of Structural Geology 17, 1139–1149.
Farr, T.G., Rosen, P.A., Caro, E., Crippen, R., Duren, R., Hensley, S., Kobrick, M., Paller, M., Rodriguez, E., Roth, L., Seal, D., Shaffer, S., Shimada, J., Umland, J., Werner, M., Oskin, M., Burbank, D., Alsdorf, D., 2007. The shuttle radar topography mission. Reviews of Geophysics 45.
Fildani, A., Hessler, A.M., 2005. Stratigraphic record across a retroarc basin inversion: Rocas Verdes–Magallanes Basin, Patagonian Andes, Chile. Geological Society of America Bulletin 117, 1596.
Fildani, A., Cope, T.D., Graham, S.A., Wooden, J.L., 2003. Initiation of the Magallanes foreland basin: timing of the southernmost Patagonian Andes orogeny revised by detrital zircon provenance analysis. Geology 31, 1081.
Fosdick, J.C., Romans, B.W., Fildani, A., Bernhardt, A., Calderon, M., Graham, S.A., 2011. Kinematic evolution of the Patagonian retroarc fold-and-thrust belt and Magallanes foreland basin, Chile and Argentina, 51 30′S. Geological Society of America Bulletin 123, 1679–1698.
Gartrell, A., Hudson, C., Evans, B., 2005. The influence of basement faults during extension and oblique inversion of the Makassar Straits rift system: insights from analog models. AAPG Bulletin 89, 495–506.
Ghiglione, M., Ramos, V.A., 2005. Progression of deformation and sedimentation in the southernmost Andes. Tectonophysics 405, 25–46.
Ghiglione, M.C., Suarez, F., Ambrosio, A., Da Poian, G., Cristallini, E.O., Pizzio, M.F., Reinoso, R.M., 2009. Structure and evolution of the austral basin fold-thrust belt, Southern Patagonian Andes. Revista de la Asociación Geológica Argentina 65, 215–226.
Ghiglione, M.C., Quinteros, J., Yagupsky, D., Bonillo-Martínez, P., Hlebszevtich, J., Ramos, V.A., Vergani, G., Figueroa, D., Quesada, S., Zapata, Y.T., 2010. Structure and tectonic history of the foreland basins of southernmost South America. Journal of South American Earth Sciences 29, 262–277.
Ghiglione, M.C., Navarrete-Rodríguez, A.T., González-Guillot, M., Bujalesky, G., 2013. The opening of the Magellan Strait and its geodynamic implications. Terra Nova 25, 13–20.
Giacosa, R., Fracchia, D., Heredia, N., 2012. Structure of the Southern Patagonian Andes at 49°S, Argentina. Geologica Acta 10, 1–19.
Giambiagi, L., 2003. The control of pre-existing extensional structures on the evolution of the southern sector of the Aconcagua fold and thrust belt, southern Andes. Tectonophysics 369, 1–19.
Gibbs, A.D., 1984. Structural evolution of extensional basin margins. Journal of the Geological Society 141, 609–620.
Hervé, F., 1988. Late Paleozoic subduction and accretion in Southern Chile. Episodes 11, 183–188.
Hubbert, M.K., 1937. Theory of scaled models as applied to the study of geological structures. Geological Society of America Bulletin 48, 1459–1519.
Hubbert, M.K., 1951. The mechanical basis for certain familiar geologic structures. Geological Society of America Bulletin 62, 355.
Huyghe, P., Mugnier, J.-L., 1992. The influence of depth on reactivation in normal faulting. Journal of Structural Geology 14, 991–998.
Jacques, J., 2003. A tectonostratigraphic synthesis of the Sub-Andean basins: implications for the geotectonic segmentation of the Andean Belt. Journal of the Geological Society 160, 687–701.
Kley, J., Monaldi, C.R., 2002. Tectonic inversion in the Santa Barbara System of the central Andean foreland thrust belt, northwestern Argentina. Tectonics 21.
Kley, J., Monaldi, C.R., Salfity, J.A., 1999. Along-strike segmentation of the Andean foreland: causes and consequences. Tectonophysics 301, 75–94.
Konstantinovskaya, E.A., Harris, L.B., Poulin, J., Ivanov, G.M., 2007. Transfer zones and fault reactivation in inverted rift basins: insights from physical modelling. Tectonophysics 441, 1–26.
Koopman, A., Speksnijder, A., Horsfield, W.T., 1987. Sandbox model studies of inversion tectonics. Tectonophysics 137, 379–388.
Kraemer, P.E., 1994. Segmentación geológica y geofísica en los Andes Patagónicos. Consecuencia de discontinuidades en el rift Jurásico? Congreso Geológico Chileno, pp. 71–75.
Kraemer, P.E., 1998. Structure of the Patagonian Andes: regional balanced cross section at 50° S, Argentina. International Geology Review 40, 896–915.
Kraemer, P.E., 2003. Orogenic shortening and the origin of the Patagonian orocline (56° S. lat). Journal of South American Earth Sciences 15, 731–748.
Kraemer, P.E., Riccardi, A.C., 1997. Estratigrafía de la región comprendida entre los lagos Argentino y Viedma (49°40′–50°10′), Provincia de Santa Cruz. Revista de la Asociación Geológica Argentina 52, 333–360.
Kraemer, P.E., Ploszkiewicz, J., Ramos, V.A., 2002. Estructura de la Cordillera Patagónica Austral entre los 46 y 52 S. Geologia y Recursos Naturales de la provincia de Santa Cruz. Relatorio del 15, 353–364.
Larsen, P.H., 1988. Relay structures in a Lower Permian basement-involved extension system, East Greenland. Journal of Structural Geology 10, 3–8.
Limeres, M., Dellape, D., 2005. Formacion Mata Amarilla: Descubrimiento de Petróleo al Norte del río Santa Cruz, Cuenca Austral, Argentina. 5° Congreso De Exploración De Hidrocarburos.
Macellari, C.E., Barrio, C.A., Manassero, M.J., 1989. Upper cretaceous to paleocene depositional sequences and sandstone petrography of southwestern Patagonia (Argentina and Chile). Journal of South American Earth Sciences 2, 223–239.
Manassero, M., 1988. Petrografía y procedencia de las areniscas cretácicas superiores de la Cuenca Austral, Argentina. Revista de la Asociación Geológica Argentina 43, 175–187.
Marinelli, R., 1998. Reservorios deltaicos de la Formación Piedra Clavada. Boletín de Informaciones Petroleras 15, 28–37.
McClay, K.R., 1989. Analogue models of inversion tectonics. Geological Society, London, Special Publications 44, 41–59.
McClay, K.R., 1990. Extensional fault systems in sedimentary basins: a review of analogue model studies. Marine and Petroleum Geology 7, 206–233.
McClay, K.R., 1995. Analogue modelling of orthogonal and oblique rifting. Marine and Petroleum Geology 12, 137–151.
Mitra, S., Islam, Q., 1994. Experimental (clay) models of inversion structures. Tectonophysics 230, 211–222.
Panien, M., Schreurs, G., Pfiffner, A., 2005. Sandbox experiments on basin inversion: testing the influence of basin orientation and basin fill. Journal of Structural Geology 27, 433–445.
Panien, M., Buiter, S.J.H., Schreurs, G., Pfiffner, O.A., 2006. Inversion of a symmetric basin: insights from a comparison between analogue and numerical experiments. Geological Society, London, Special Publications 253, 253–270.
Pankhurst, R.J., 2000. Episodic silicic volcanism in Patagonia and the Antarctic Peninsula: chronology of magmatism associated with the break-up of Gondwana. Journal of Petrology 41, 605–625.
Paton, D.A., Underhill, J.R., 2004. Role of crustal anisotropy in modifying the structural and sedimentological evolution of extensional basins: the Gamtoos Basin, South Africa. Basin Research 16, 339–359.
Peacock, D.C.P., Knipe, R.J., Sanderson, D.J., 2000. Glossary of normal faults. Journal of Structural Geology 22, 291–305.
Pfiffner, O.A., Ramsay, J.G., 1982. Constraints on geological strain rates: arguments from finite strain states of naturally deformed rocks. Journal of Geophysical Research 87, 311.
Ramberg, H., 1981. Gravity, Deformation and the Earth's Crust: In Theory, Experiments and Geological Application. Academic Press, London and New York, p. 452.
Ramos, V.A., 2006. Overview of the tectonic evolution of the southern Central Andes of Mendoza and Neuquén (35°–39°S latitude). In: Kay, S.M., Ramos, V.A. (Eds.), Evolution of an Andean Margin: A Tectonic and Magmatic View from the Andes to the Neuquén Basin (35°–39°S Latitude): Geological Society of America Special Paper, pp. 1–17.
Ramos, V.A., Cristallini, E.O., Introcaso, A., 2004. The Andean Thrust System — latitudinal variations in structural styles and orogenic shortening. AAPG Memoir 30–50.
Ranalli, G., 2000. Rheology of the crust and its role in tectonic reactivation. Journal of Geodynamics 30, 3–15.
Romans, B.W., Hubbard, S.M., Graham, S.A., 2009. Stratigraphic evolution of an outcropping continental slope system, Tres Pasos Formation at Cerro Divisadero, Chile. Sedimentology 56, 737–764.
Romans, B.W., Fildani, A., Graham, S.A., Hubbard, S.M., Covault, J.A., 2010. Importance of predecessor basin history on sedimentary fill of a retroarc foreland basin: provenance analysis of the Cretaceous Magallanes basin, Chile (50–52°S). Basin Research 22, 640–658.
Serra, S., Nelson, R.A., 1988. Clay modeling of rift asymmetry and associated structures. Tectonophysics 153, 307–312.
Shultz, M., Fildani, A., Cope, T., 2005. Deposition and stratigraphic architecture of an outcropping ancient slope system: Tres Pasos Formation, Magallanes Basin, southern Chile. Geological Society of London 255, 27–50.
Sibson, R.H., 1985. A note on fault reactivation. Journal of Structural Geology 7, 751–754.
Stewart, L., 1996. Behaviour of spherical rigid objects and passive markers during bulk inhomogeneous shortening of a fluid. Journal of Structural Geology 18.

Stewart, I., Hancock, P., 1991. Scales of structural heterogeneity within neotectonic normal fault zones in the Aegean region. Journal of Structural Geology 13, 191–204.
Uliana, M., Biddle, K., Cerdan, J., Tankard, A., 1989. Mesozoic extension and the formation of Argentine sedimentary basins. AAPG Special Volumes 46, 599–614.
Uliana, M., Arteaga, M.E., Legarreta, L., Cerdan, J.J., Peroni, G.O., 1995. Inversion structures and hydrocarbon occurrence in Argentina. Geological Society, London, Special Publications 88, 211–233.
Walsh, J.J., Watterson, J., 1991. Geometric and kinematic coherence and scale effects in normal fault systems. Geological Society, London, Special Publications 56, 193–203.
Weijermars, R., 1993. Pulsating strains. Tectonophysics 220, 51–67.
Wilson, T., 1991. Transition from back-arc to foreland basin development in the southernmost Andes: stratigraphic record from the Ultima Esperanza District, Chile. Geological Society of America Bulletin 103, 98–111.
Yagupsky, D., Cristallini, E.O., Fantin, J., Valcarce, G., Bottesi, G., Varade, R., 2008. Oblique half-graben inversion of the Mesozoic Neuquén Rift in the Malargüe Fold and Thrust Belt, Mendoza, Argentina: new insights from analogue models. Journal of Structural Geology 30, 839–853.
Zilli, N., Pedrazzini, M., Peroni, G.O., 2002. La Cuenca Austral. In: Haller, M. (Ed.), Geología y Recursos Naturales De Santa Cruz. 15° Congreso Geológico Argentino (El Calafate), Relatorio, pp. 607–662.